1521-0103/347/3/669–680$25.00
THE JOURNAL OF PHARMACOLOGY AND EXPERIMENTAL THERAPEUTICS

http://dx.doi.org/10.1124/jpet.113.208421
J Pharmacol Exp Ther 347:669–680, December 2013

Pharmacologic Profiling of Phosphoinositide 3-Kinase Inhibitors as Mitigators of Ionizing Radiation–Induced Cell Death[S]

John S. Lazo, Elizabeth R. Sharlow, Michael W. Epperly, Ana Lira, Stephanie Leimgruber, Erin M. Skoda, Peter Wipf, and Joel S. Greenberger

Department of Pharmacology, University of Virginia, Charlottesville, Virginia (J.S.L., E.R.S., A.L., S.L.); Departments of Radiation Oncology (M.W.E., J.S.G.), Chemistry (E.M.S., P.W.), and Pharmaceutical Sciences (P.W.), University of Pittsburgh, Pittsburgh, Pennsylvania

Received July 29, 2013; accepted September 25, 2013

ABSTRACT

Ionizing radiation (IR) induces genotoxic stress that triggers adaptive cellular responses, such as activation of the phosphoinositide 3-kinase (PI3K)/Akt signaling cascade. Pluripotent cells are the most important population affected by IR because they are required for cellular replenishment. Despite the clear danger to large population centers, we still lack safe and effective therapies to abrogate the life-threatening effects of any accidental or intentional IR exposure. Therefore, we computationally analyzed the chemical structural similarity of previously published small molecules that, when given after IR, mitigate cell death and found a chemical cluster that was populated with PI3K inhibitors. Subsequently, we evaluated structurally diverse PI3K inhibitors. It is remarkable that 9 of 14 PI3K inhibitors mitigated γIR-induced death in pluripotent NCCIT cells as measured by caspase 3/7 activation. A single intraperitoneal dose of LY294002 [2-(4-morpholinyl)-8-phenyl-4*H*-1-benzopyran-4-one], administered to mice at 4 or 24 hours, or PX-867 [(4*S*,4*aR*,5*R*,6*aS*,9*aR*,*Z*)-11-hydroxy-4-(methoxymethyl)-4*a*,6*a*-dimethyl-2,7,10-trioxo-1-(pyrrolidin-1-ylmethylene)-1,2,4,4*a*,5,6,6*a*,7,8,9,9*a*,10-dodecahydroindeno[4,5-*H*]isochromen-5-yl acetate (CID24798773)], administered 4 hours after a lethal dose of γIR, statistically significantly ($P < 0.02$) enhanced in vivo survival. Because cell cycle checkpoints are important regulators of cell survival after IR, we examined cell cycle distribution in NCCIT cells after γIR and PI3K inhibitor treatment. LY294002 and PX-867 treatment of nonirradiated cells produced a marked decrease in S phase cells with a concomitant increase in the G_1 population. In irradiated cells, LY294002 and PX-867 treatment also decreased S phase and increased the G_1 and G_2 populations. Treatment with LY294002 or PX-867 decreased γIR-induced DNA damage as measured by γH2AX, suggesting reduced DNA damage. These results indicate pharmacologic inhibition of PI3K after IR abrogated cell death.

Introduction

Humans are continuously exposed to low-level ionizing radiation (IR) from natural sources. Consumer, industrial, and medical applications of IR add to our exposure. Events such as the Three Mile Island, Chernobyl, and Fukushima Daiichi accidents dramatically underscore the potential dangers of an accidental IR overexposure to the public. Furthermore, we cannot exclude the possibility that radioactive materials could be exploited as weapons. Regrettably, there are no established clinically effective pharmacologic strategies to intervene once an individual or a population has been exposed to IR.

Whole-body IR doses of approximately 1–8 Gy produce physiologic changes collectively known as acute radiation syndrome (Hall and Giaccia, 2006; Greenberger et al., 2011). One of the major mortality factors associated with acute radiation syndrome is damage to the hematopoietic and intestinal progenitor cells, which share many properties with pluripotent stem cells (Wang et al., 2009; Sokolov et al., 2011). Unfortunately, progenitor cells are not a facile model system

This work was supported by the National Institutes of Health National Institute of Allergy and Infectious Diseases [Grant U19 AI068021].
dx.doi.org/10.1124/jpet.113.208421.
[S] This article has supplemental material available at jpet.aspetjournals.org.

ABBREVIATIONS: A66, (2*S*)-*N*1-(5-(2-tert-butylthiazol-4-yl)-4-methylthiazol-2-yl)pyrrolidine-1,2-dicarboxamide; ANOVA, analysis of variance; ACE, angiotensin-converting enzyme; AS-605240, (*Z*)-5-(quinoxalin-6-ylmethylene)thiazolidine-2,4-dione); BEZ-235, 2-methyl-2-(4-(3-methyl-2-oxo-8-(quinolin-3-yl)-2,3-dihydroimidazo[4,5-c]quinolin-1-yl)phenyl)propanenitrile; CAL-101, (*S*)-2-(1-(9*H*-purin-6-ylamino)propyl)-5-fluoro-3-phenylquinazolin-4(3*H*)-one; DMSO, dimethylsulfoxide; EdU, 5-ethynyl-2′-deoyuridine; FBS, fetal bovine serum; GDC-0980, (*S*)-1-(4-((2-(2-aminopyrimidin-5-yl)-7-methyl-4-morpholinothieno[3,2-day]pyrimidin-6-yl)methyl)piperazin-1-yl)-2-hydroxypropan-1-one; GSK2126458, 2,4-difluoro-*N*-(2-methoxy-5-(4-(pyridazin-4-yl)quinolin-6-yl)pyridin-3-yl)benzenesulfonamide; GSK3, glycogen synthase kinase 3; HMG-CoA, 3-hydroxy-3-methylglutaryl coenzyme A; IR, ionizing radiation; LY294002, 2-(4-morpholinyl)-8-phenyl-4*H*-1-benzopyran-4-one; mTOR, mammalian target of rapamycin; palomid 529, 3-(4-methoxybenzyloxy)-8-(1-hydroxyethyl)-2-methoxy-6*H*-benzo[c]chromen-6-one; PI-103, phenol, 3-[4-(4-morpholinyl)pyrido[3′,2′:4,5]furo[3,2-day]pyrimidin-2-yl]-phenol; PI3K, phosphoinositide 3-kinase; PX-867, (4*S*,4*aR*,5*R*,6*aS*,9*aR*,*Z*)-11-hydroxy-4-(methoxymethyl)-4*a*,6*a*-dimethyl-2,7,10-trioxo-1-(pyrrolidin-1-ylmethylene)-1,2,4,4*a*,5,6,6*a*,7,8,9,9*a*,10-dodecahydroindeno[4,5-*H*]isochromen-5-yl acetate (CID24798773); siRNA, small interfering RNA; XL-147, *N*-(3-(benzo[c][1,2,5]thiadiazol-5-ylamino)quinoxalin-2-yl)-4-methylbenzenesulfonamide; ZSTK474, 2-(difluoromethyl)-1-(4,6-dimorpholino-1,3,5-triazin-2-yl)-1*H*-benzo[d]imidazole.

for the study of radiation response in culture. Therefore, we (Zellefrow et al., 2012) and others (Wang et al., 2009) have searched for and identified an immortalized pluripotent human cell line, NCCIT, that has cell cycle characteristics and radiobiologic sensitivity relevant to the key targeted human populations: hematopoietic and gut progenitor cells. We recently optimized the NCCIT pluripotent progenitor cell model for a high-throughput screening assay based on small interfering RNA (siRNA) in an effort to identify novel signaling pathways involved in cellular survival after irradiation (Zellefrow et al., 2012). Our preliminary analysis surprisingly suggested an enabling involvement of the phosphoinositide 3-kinase (PI3K) pathway in IR-mediated cell death (Zellefrow et al., 2012).

The initial mediators of cellular damage after IR exposure are short-lived reactive oxygen species, which lead to damage to DNA, proteins, lipids, and other macromolecules (Hall and Giaccia, 2006). Multicellular organisms have evolved with multiple adaptive damage responses that enable them to constructively address the damage associated with low radiation exposure. These include the enlistment of elaborate DNA repair processes, activation of cell cycle checkpoints to block the replication of damaged DNA or cytokinesis, modification of transcription, upregulation of antioxidants, promotion of autophagy, and engagement of cellular senescence or differentiation pathways. Failure to resolve IR-induced damage generally leads to the activation of apoptotic cell death processes. The existence of adaptive signaling responses to the radiation-induced damage implies that pharmacologic targets might exist, allowing for some mitigation of the toxic effects of radiation, especially after exposure to low doses. Although some experimental radiomitigators have been reported (Citrin et al., 2010; Epperly et al., 2010; Johnson et al., 2010; Greenberger et al., 2011; Kim et al., 2011; Moulder et al., 2011; Zellefrow et al., 2012), the mechanisms of mitigation are not well defined, and none of the early generation compounds have yet been clinically validated, recognizing that this is an ethical challenge.

The PI3K pathway controls many processes, including apoptosis, the most common form of programmed cell death, and upregulation of the PI3K/Akt pathway has been observed in response to genotoxic damage (Brognard et al., 2001; Viniegra et al., 2005). Increased PI3K activity is commonly observed in tumor cells, and PI3K inhibition before chemotherapy or radiotherapy often, but not always, increases tumor cell death (Viniegra et al., 2005; Courtney et al., 2010; Firat et al., 2012; Laplante and Sabatini, 2012). Much less is known about the fate of cells when PI3K is inhibited after IR exposure. We now demonstrate reduced pluripotent cell death with multiple small molecule PI3K inhibitors administered after IR treatment as well as increased in vivo survival with two PI3K inhibitors, thus expanding the evidence for a unique and paradoxical role of the PI3K pathway in radiation toxicity. Mechanistically, we find prototype PI3K inhibitors reduced the S phase population, induced a transient G_1 and G_2/M phase arrest, and decreased DNA damage, which could mediate the enhanced survival.

Materials and Methods

Reagents. CaspaseGlo 3/7 caspase activity assays were purchased from Promega (Madison, WI). White and black tissue culture treated 384-well microtiter plates were from Greiner Bio-One (Frickenhausen, Germany) and six-well plates from Corning (Corning, Inc., NY). RPMI-1640 medium and fetal bovine serum (FBS) were from Media-Tech, Inc. (Manassas, VA). Unless otherwise noted, reagents were purchased from Sigma-Aldrich (St. Louis, MO). LY294002 (2-(4-morpholinyl)-8-phenyl-4*H*-1-benzopyran-4-one) was obtained from Enzo Life Sciences (Farmingdale, NY) and annexin V from BD Biosciences (San Jose, CA). A66 [(2*S*)-*N*1-(5-(2-tert-butylthiazol-4-yl)-4-methylthiazol-2-yl)pyrrolidine-1,2-dicarboxamide]; PI-103 (phenol, 3-[4-(4-morpholinyl)pyrido[3′,2′:4,5]furo[3,2-day]pyrimidin-2-yl]-phenol); palomid 529 [3-(4-methoxybenzyloxy)-8-(1-hydroxyethyl)-2-methoxy-6*H*-benzo[c]chromen-6-one]; GSK2126458 [2,4-difluoro-*N*-(2-methoxy-5-(4-(pyridazin-4-yl)-quinolin-6-yl)pyridin-3-yl)benzenesulfonamide]; CAL-101 [(*S*)-2-(1-(9*H*-purin-6-ylamino)propyl)-5-fluoro-3-phenylquinazolin-4(3*H*)-one]; AS-605240 [(*Z*)-5-(quinoxalin-6-ylmethylene)thiazolidine-2,4-dione)]; and AS-252424 [(*Z*)-5-((5-(4-fluoro-2-hydroxyphenyl)furan-2-yl)methylene)thiazolidine-2,4-dione] were from Selleckchem (Toledo, OH). BEZ-235 [2-methyl-2-(4-(3-methyl-2-oxo-8-(quinolin-3-yl)-2,3-dihydroimidazo[4,5-c]quinolin-1-yl)phenyl)propanenitrile] and ZSTK474 [2-(difluoromethyl)-1-(4,6-dimorpholino-1,3,5-triazin-2-yl)-1*H*-benzo[d]imidazole] were purchased from LC Laboratories (Woburn, MA). XL-147 [*N*-(3-(benzo[c][1,2,5]thiadiazol-5-ylamino)quinoxalin-2-yl)-4-methylbenzenesulfonamide] and GDC-0980 [(*S*)-1-(4-((2-(2-aminopyrimidin-5-yl)-7-methyl-4-morpholinothieno[3,2-day]pyrimidin-6-yl)methyl)piperazin-1-yl)-2-hydroxypropan-1-one] were obtained from Active Biochemicals (Hong Kong). Antibodies for use in Western blotting against GSK3, pGSK3 Ser21/9, Akt, pAkt Ser473, and γH2AX were purchased from Cell Signaling Technologies (Danvers, MA). PX-867 [(4*S*,4*aR*,5*R*,6*aS*,9*aR*,*Z*)-11-hydroxy-4-(methoxymethyl)-4*a*,6*a*-dimethyl-2,7,10-trioxo-1-(pyrrolidin-1-ylmethylene)-1,2,4,4*a*,5,6,6*a*,7,8,9,9*a*,10-dodecahydroindeno[4,5-*H*]isochromen-5-yl acetate, CID24798773] was synthesized as previously described elsewhere (Wipf et al., 2004; Wipf and Halter, 2005).

Cell Culture. Human pluripotent embryonal carcinoma NCCIT and NTERA2 cells, which were each isolated from an adult male, were purchased from the American Type Culture Collection (Manassas, VA). Cells were maintained in RPMI-1640 (NCCIT) or Dulbecco's modified Eagle's medium (NTERA2) supplemented with 10% fetal bovine serum (FBS), penicillin, streptomycin, and 2 mM L-glutamine and were maintained at 37°C with 5% CO_2. Cells were carried for ≤10 passages, at which time new cells were thawed from our frozen stocks. Cells were routinely monitored for mycoplasma and found negative.

Western Blotting. Protein lysates from NCCIT cells were isolated as previously described elsewhere (Thaker et al., 2010; Zellefrow et al., 2012) and loaded (~10–50 μg/well) on a 4–12% acrylamide gradient gel for protein separation. The proteins were transferred to a polyvinylidene difluoride membrane using an iBlot system (Invitrogen, Carlsbad, CA). The membranes were blotted in PBS containing 0.1% Tween 20 with Odyssey Blocking Buffer (Li-Cor, Lincoln, NE) diluted 1:2 (vol:vol) at 4°C overnight with the following antibodies: anti-GSK3, anti-pGSK3, anti-Akt, anti-pAkt, γH2AX, and GAPDH. Positive antibody reactions were visualized using goat anti-rabbit DyLight 680 or 800 (Thermo Fisher Scientific, Waltham, MA). Membranes were imaged using a Li-Cor Odyssey scanner, and bands were analyzed using Odyssey 3.0 analytical software (Li-Cor).

Caspase 3/7 and Membrane Permeability Assays. To determine radiation mitigation, we assayed caspase 3/7 activity in vehicle and compound-treated cells using a previously described assay (Zellefrow et al., 2012), which was modified to enhance reproducibility. In brief, we seeded 3500 cells/well in 384-well microtiter plates after receiving 0 or 4 Gy γIR using a J.L. Shepherd Mark 1 cesium irradiator (J.L. Shepherd & Associates, San Fernando, CA), which is maintained and calibrated by the University of Virginia Department of Environmental Health and Safety. After 1 hour of incubation at 37°C, dimethylsulfoxide (DMSO) vehicle control or PI3K inhibitors were added to the cells at the indicated concentrations. After a 47-hour incubation at 37°C, CaspaseGlo 3/7 reagent (Promega) was added into the wells. After a 1-hour incubation at room temperature, the luminescence was measured on a Molecular Devices

SpectraMax M5 plate reader (Sunnyvale, CA). For some studies CellTox Green cytotoxicity reagent (Promega) was used as recommended by the manufacturer.

Flow Cytometry Assay. NCCIT cells were exposed to 0 or 4 Gy γIR as a single-cell suspension in a 50-ml conical tube and then plated in six-well plates at a density of 2×10^5 cells/well. After 1 hour, DMSO vehicle, LY294002 (6.25 μM), or PX-867 (0.63 μM) were added and incubated for the indicated time. Cell cycle distribution was determined using the Click-iT EdU Alexa Fluor 488 Flow Cytometry Assay Kit (Invitrogen) and FxCycle Far Red DNA stain (Invitrogen). Cells were treated with 10 μM 5-ethynyl-2′-deoxyuridine (EdU) 6 hours before harvesting. Data acquisition was performed with FACSCalibur Benchtop Analyzer (Becton Dickinson, San Jose, CA) and CellQuest (Becton Dickinson) software. The data were analyzed using FlowJo software (TreeStar, Inc., Ashland, OR).

Three-Dimensional Chemical Structural Analysis. To determine the structural similarity of known and novel radiation mitigators, we performed a three-dimensional (3D) similarity analysis (http://pubchem.ncbi.nim.nih.gov/) based on the single linkage algorithm (Olson, 1995). Briefly, identifiers for each compound were accessed from the Pubchem database (i.e., Pubchem CIDs). For each parental chemotype, up to 10 conformers were calculated. If a particular chemotype had no 3D conformers, the parental chemotypes were used to determine 3D conformer similarity. Structural clustering was based on the parental chemotypes, with the most similar conformer pairs used to represent a pair of compounds when conformer sets were compared. For calculations of 3D similarity, 3D superposition was optimized by shape with 3D similarity based on the sum of the shape and feature similarity scores. Similarity scores of ≥1.03 using up to 10 calculated conformers were considered statistically significantly different (Kim et al., 2012). This threshold score was derived from 2 S.D. from the mean of the shape-Tanimoto-optimized combo-Tanimoto average of 0.77 ± 0.13 (S.D.) (Kim et al., 2012). Thus, it provides the 95% confidence limit when using 10 diverse conformers.

In Vivo Mitigation Assays. The in vivo mitigation assays were performed as previously described elsewhere (Rwigema et al., 2011; Zellefrow et al., 2012). C57BL/6NTac female mice (15 mice/treatment group) were irradiated to 9.25 Gy and injected i.p. with LY294002 (30 mg/kg; 98 μmol/kg), PX-867 (30 mg/kg; 60 μmol/kg), or the vehicle control 4 or 24 hours later. The compounds were dissolved in 0.1 volume of ethanol followed by the addition of 0.1 volume of Cremophor EL, vortexing, and the addition of 0.8 volumes of distilled water to a final concentration of 6 mg/ml. Mice were observed for the development of the hematopoietic syndrome, at which time they were sacrificed. The hematopoietic syndrome in humans is characterized by nausea, vomiting, anorexia, lethargy, destruction of the bone marrow, and atrophy of the spleen and lymph nodes. Mice exhibit all

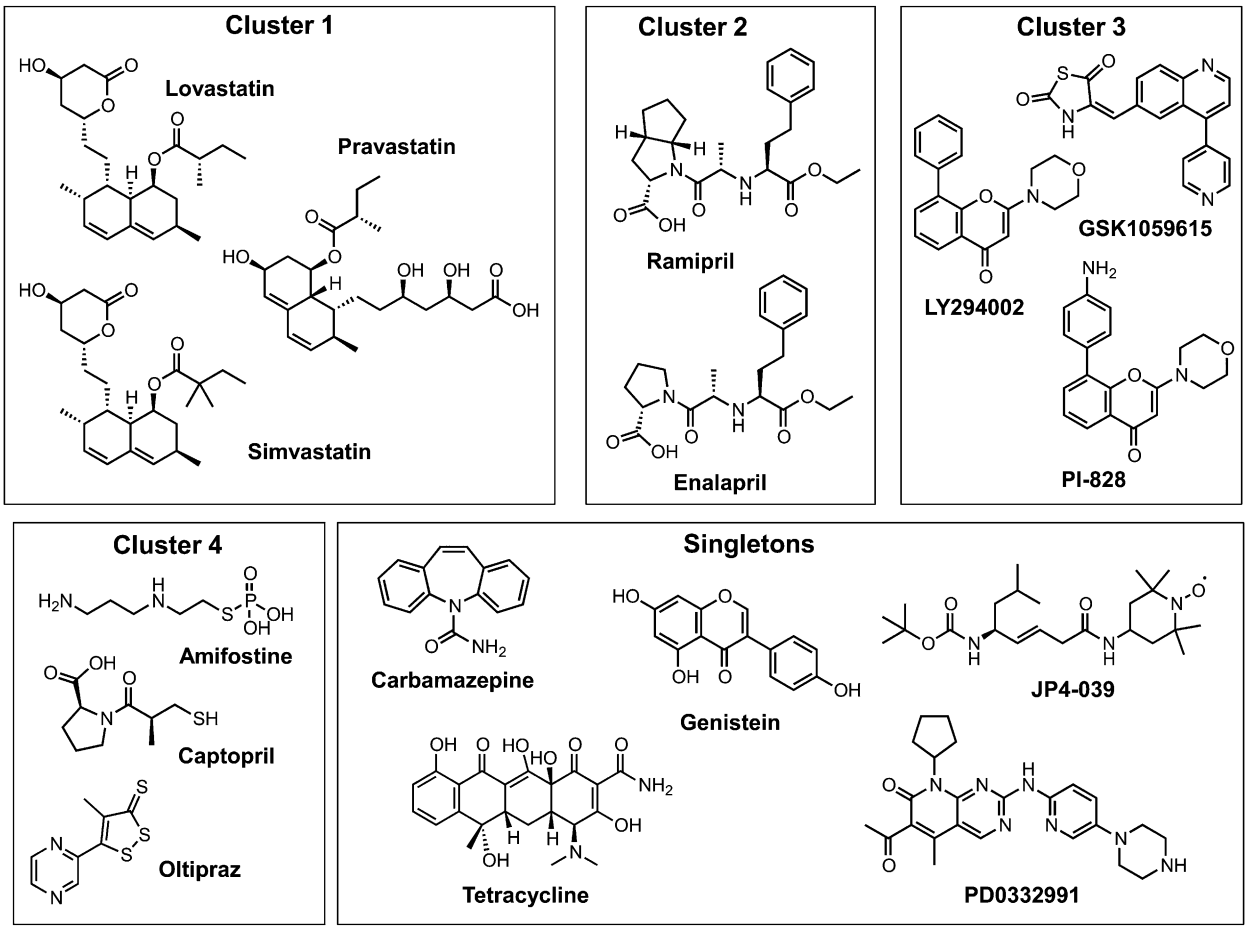

Fig. 1. Structural clustering of known radiation mitigators. Previously published radiation mitigators (Epperly et al., 2010; Greenberger et al., 2011; Moulder et al., 2011; Zellefrow et al., 2012) were subjected to 3D similarity analyses (http://pubchem.ncbi.nim.nih.gov/) based on the single linkage algorithm (Olson, 1995). For calculations of 3D similarity, 3D superposition was optimized by shape, with 3D similarity based on the sum of the shape and feature similarity scores. Compounds were considered similar if their similarity score was ≥1.03 using up to 10 calculated conformers. Subsequently, compounds in the singleton bin were further analyzed based on chemical pharmacophore considerations, and cluster 4 was generated to combine active thiols and thiol precursors. Pravastatin was moved into cluster 1 because of the shared hexahydronaphthalene (decalin) and ester moieties.

of these symptoms except nausea or vomiting. The specific characteristics we used to decide when to sacrifice the mice were lethargy, loss of greater than 20% of their body weight, hunching of back, and ruffling of fur. For in vivo studies, the irradiator is a J.L. Shepherd Mark I cesium irradiator. The calibration is checked every 3 months via dosimeter by the University of Pittsburgh Radiation Safety Office.

Statistical Analysis. Data were expressed as the mean ± S.E.M. of at least three determinations. Data from the in vitro radiation survival curves were analyzed with Student's t test, and the mouse survival data were analyzed by a log-rank test (Epperly et al., 2010). Statistical comparisons between different groups were performed with Student's t test or analysis of variance (ANOVA). $P \leq 0.05$ was considered statistically significant.

Animal Welfare. The University of Pittsburgh Institutional Animal Care and Use Committee approved the animal protocol (no. 1201406), and the experiments were performed under the supervision of the Division of Laboratory Animal Research of the University of Pittsburgh. The Division of Laboratory Animal Research of the University of Pittsburgh provided veterinary care.

Results

Structural Similarity Analysis of Known Radiation Mitigators. At least 16 compounds have previously been reported to mitigate the toxic effects of IR in a variety of in vitro model systems (Citrin et al., 2010; Epperly et al., 2010; Johnson et al., 2010; Greenberger et al., 2011; Moulder et al., 2011; Zellefrow et al., 2012). The mechanisms by which these compounds reduce the toxic effects of IR are poorly defined. Recognizing that chemical similarity analyses can provide rich information about core bioactive chemotypes and potential molecular targets (Welsch et al., 2010; Ma et al., 2011), we subjected 16 of the known radiation mitigators to a 3D chemical similarity analysis as defined by a value of ≥1.03 (Olson, 1995). Three chemical clusters and seven less closely related compounds were identified. In addition, we grouped pravastatin together with lovastatin and simvastatin into cluster 1 because of the presence of the closely related decalin ester pharmacophores in these molecules, which are commonly thought to primarily act by inhibition of 3-hydroxy-3-methylglutaryl coenzyme A (HMG-CoA) reductase to reduce low-density lipoprotein cholesterol levels (Fig. 1). Cluster 2 contained angiotensin-converting enzyme (ACE) inhibitors. It is interesting that another structurally unrelated ACE inhibitor, captopril, was observed among the computationally obtained singletons; this compound, amifostine, and oltipaz were subsequently moved into a newly defined cluster 4, which contained active thiols or prodrug/precursors of thiols, leaving five structurally diverse singletons (Fig. 1). Interestingly, the

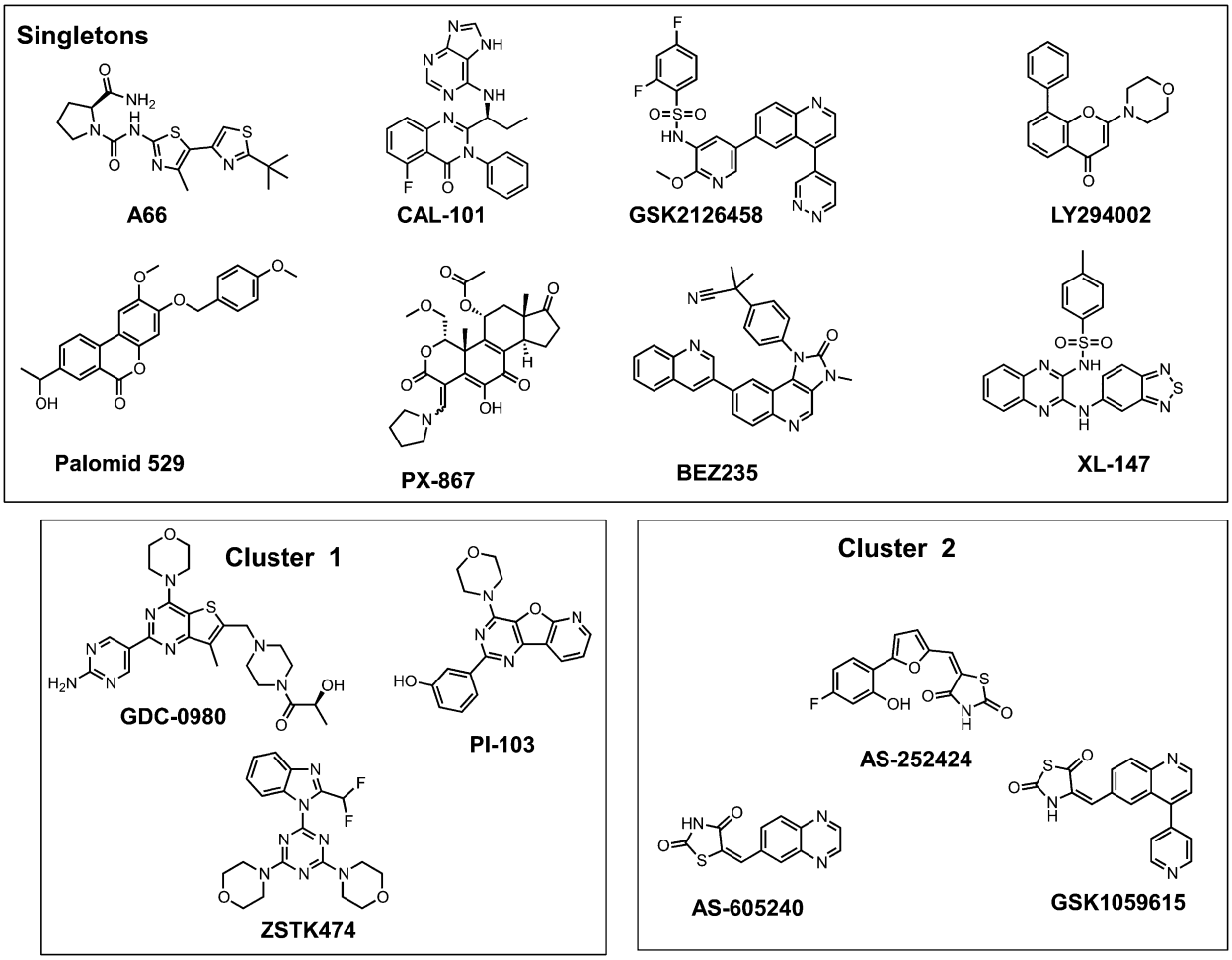

Fig. 2. Structural clustering of PI3K radiation mitigators. Previously reported PI3K inhibitors were selected for a 3D similarity search by cluster analysis, as described in Fig. 1.

remaining cluster 3 contained three known inhibitors of the PI3K/Akt pathway, which controls cell growth.

We subsequently assembled a group of 14 PI3K inhibitors and examined them using the pluripotent NCCIT cell apoptosis model (Zellefrow et al., 2012). These inhibitors were structurally diverse with the exception of the thiazolidinedione cluster 2, which contained AS-605240, AS-252424, and GSK1059615 (Fig. 2). Four PI3K inhibitors, A66, CAL-101, palomid-529, and XL-147, were inactive at the concentrations tested, whereas GSK2126458 was toxic to nonirradiated and irradiated cells (Supplemental Fig. 1). As indicated in Fig. 3, it is striking that 9 (64%) of the 14 PI3K inhibitors mitigated IR-induced caspase 3/7 activation. This is particularly surprising and even paradoxical as the PI3K pathway is most commonly associated with tumor cell survival, especially with toxic substances (Courtney et al., 2010). We previously observed mitigation of annexin V externalization with LY294002 and NCCIT cells (Zellefrow et al., 2012), suggesting this phenomenon was not a artifact of the assay. Furthermore, we observed LY294002 mitigation of IR-induced loss of replicative capacity with another cell population, 32D 3cl cells, indicating it was not unique to NCCIT cells (Zellefrow et al., 2012). We also observed mitigation of IR-induced caspase 3/7 with AS-25242 and another human progenitor cell line, NTERA2 (Supplemental Fig. 1F). Low doses of IR generally do not initially produce marked necrosis. Thus, with IR we saw no significant change in membrane integrity, which occurs with necrotic cell death, and none of the PI3K inhibitors that produce mitigation of apoptosis cause enhanced membrane permeability (Supplemental Fig. 2, A–I). Therefore, we investigated further the potential mechanism for this radiation mitigation.

IR Rapidly but Transiently Activates the PI3K Pathway in NCCIT Cells. Previous studies have documented that even low doses of IR cause sufficient genotoxic stress to activate cellular signaling pathways, including a number of PI3K and PI3K-like kinases such as ataxia telangiectasia mutated (ATM), ataxia telangiectasia mutated and Rad3 related (ATR), and DNA-dependent protein kinase (DNA-PK), resulting in the phosphorylation of Akt on Ser473 and its activation (Brognard et al., 2001; Viniegra et al., 2005). Pluripotent NCCIT cells, when exposed to 4 Gy of γIR, produced a modest but reproducible ($P < 0.05$) increase in Akt Ser473 phosphorylation within 30 minutes (Fig. 4, A and B). Consistent with a tightly regulated signaling system, Akt activation was transient in NCCIT cells, and within 3 hours after γIR exposure the Ser473 phospho-Akt levels returned essentially to those seen under basal conditions (Figs. 4, C and D, 5A, and 6A).

We were also unable to detect reproducible phosphorylation and activation of more distal effectors of the PI3K pathway mediated by mammalian target of rapamycin (mTOR), namely, phosphorylation of Ser21 on glycogen synthase kinase 3α (GSK3α) and Ser9 on glycogen synthase kinase 3β (GSK3β) between 3 and 24 hours after γIR (Fig. 4, C and D, 5, C and E,

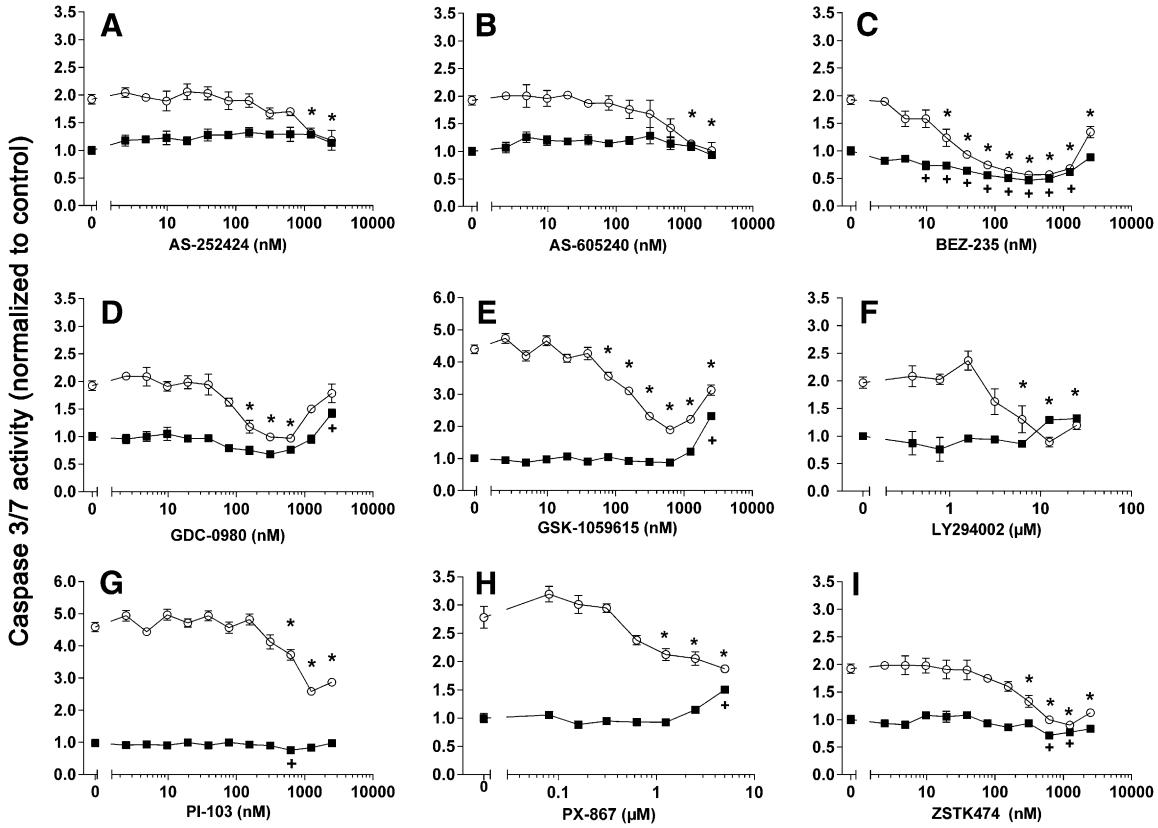

Fig. 3. The PI3K inhibitors LY294002 and PX-867 reduce radiation-induced apoptosis. NCCIT cells were exposed to 0 (■) or 4 (○) Gy γIR and 1 hour later were treated with 0.1% DMSO vehicle control or various concentrations of AS-252424 (A), AS-605240 (B), BEX-235 (C), GDC-0980 (D), GSK-1059615 (E), LY294002 (F), PI-103 (G), PX-867 (H), and ZSTK474 (I). After 48 hours, caspase 3/7 activity was determined. $N = 3$. Bars = S.E.M. Data analyzed by ANOVA. $^{*}P < 0.05$ between 4 Gy γIR exposed cells treated with DMSO vehicle or the PI3K inhibitor. $^{+}P < 0.05$ between nonirradiated cells treated with DMSO vehicle or PI3K inhibitor, which would represent compound-related apoptotic effects.

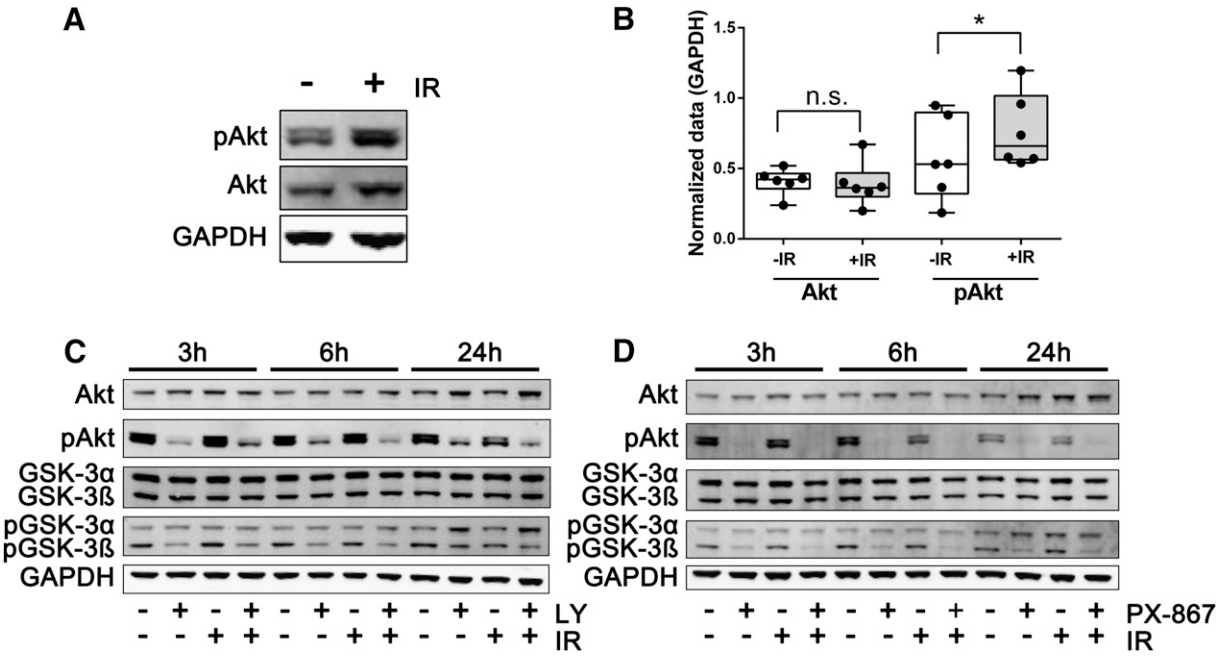

Fig. 4. Transient induction of Akt after IR and PI3K pathway inhibition by LY294002 and PX-867. NCCIT cells were exposed to 0 or 4 Gy γIR. (A) Cells were harvested 30 minutes later for Western blot analysis for Akt Ser473 phosphorylation (pAkt) and total Akt and GAPDH levels. (B) Quantification of integrative band intensities of pAkt and Akt levels 30 minutes after 0 or 4 Gy IR. Densitometry data were acquired with a Li-Cor Odyssey imaging system and normalized using GAPDH. Data were from six independent experiments analyzed using a pair Student's t test. $^*P < 0.05$. NS, not statistically significant. Representative Western blots from lysates of cells treated 1 hour after 0 or 4 Gy γIR with vehicle or 6.25 μM LY294002 (LY) (C) or 630 nM PX-867 (D) and incubated for an additional 2, 5, or 23 hours.

and 6, C and E). The protein expression levels of Akt, GSK3α, and GSK3β also remained unaltered for at least 24 hours after γIR (Figs. 4–6).

The reversible pan-PI3K inhibitor LY294002 produced sustained >60% suppression of Akt activation as indicated by Ser473 phosphorylation for at least 24 hours (Figs. 4–6) in nonirradiated and irradiated cells. LY294002 also caused a profound (>50%) suppression of GSK3α Ser21 phosphorylation and of GSK3β Ser9 phosphorylation for at least 24 hours in irradiated cells (Figs. 4C and 5, C and E). In addition, we examined the structurally distinct PX-867 (Fig. 2), which is one of 120 wortmannin analogs that we previously synthesized for improved physicochemical, pharmacokinetic, and pharmacodynamic properties (Wipf et al., 2004). PX-867 was among the most stable analogs, and, similar to wortmannin, was an irreversible PI3K inhibitor (Wipf et al., 2004). Similar to LY294002, PX-867 produced sustained suppression of Akt activation as indicated by the >50% reduction in Ser473 phosphorylation (Figs. 4D and 6A) in nonirradiated and irradiated cells. Similarly, PX-867 reduced GSK3α Ser21 phosphorylation and GSKβ Ser9 phosphorylation between 3 and 24 hours after γIR (Fig. 6, C and E) without altering the levels of these proteins (Fig. 6, D and F). PX-867 also abrogated radiation-induced caspase 3/7 activation, although over a relatively narrow nontoxic concentration range (Fig. 3H).

In Vivo Radiation Mitigation by PI3K Inhibitors. We next directly compared the in vivo radiation mitigation activity of LY294002 and PX-867 in a well-established mouse model (Greenberger et al., 2011; Zellefrow et al., 2012). A single intraperitoneal dose of LY294002 (30 mg/kg, 98 μmol/kg) administered either 4 or 24 hours after a lethal 9.25 Gy dose of γIR significantly increased survival ($P < 0.001$) (Fig. 7). In preliminary studies, we determined that the maximally tolerated intraperitoneal dose of PX-867 was 30 mg/kg (data not shown). Similar to LY294002, a single dose of PX-867 (30 mg/kg, 60 μmol/kg) administered 4 hours after 9.25 Gy statistically significantly ($P < 0.017$) increased survival (Fig. 7). Administration of a single 30 mg/kg dose of PX-867 24 hours after 9.25 Gy γIR resulted in 20% of mice surviving for 40 days, which approximated the value for 4-hour administration; however, unlike treatment with LY294002, the survival difference with vehicle treatment ($P = 0.08$) did not reach our goal for statistical significance. It is possible that this difference with LY294002 can be attributed to the lower molar dosage of PX-867 used or to the irreversible nature of the PI3K inhibition produced by PX-867. Nonetheless, these results with a single compound injection support the potential value of suppressing components of the PI3K pathway after γIR exposure.

Inhibition of the PI3K Pathway Enforces a G_1 and G_2 Phase Arrest after Irradiation. Nonirradiated NCCIT cells such as embryonic stem cells (Wang et al., 2009; Sokolov et al., 2011) maintained a high percentage (76%) of the total population in S phase with 20 and 4% in G_1 and G_2/M phase, respectively (Fig. 8 and 9). After 4 Gy γIR, NCCIT cells exhibited a prominent but transient G_2 phase arrest (Fig. 8 and 9). Twenty-eight hours after γIR, 50 ± 5% (S.E.M.; $N = 3$) of the total population remained in the G_2/M phase; by 48 hours, it decreased to 12.7 ± 0.3% (S.E.M.; $N = 3$) (Fig. 8). The G_1 phase cells comprised 15 ± 1% and 17 ± 2% of the total population 28 and 48 hours after γIR, respectively.

Treatment of nonirradiated cells with a radiation mitigation concentration (6.25 μM) of LY294002 increased the G_1 phase population at 28 hours to 49 ± 3% and decreased the S phase

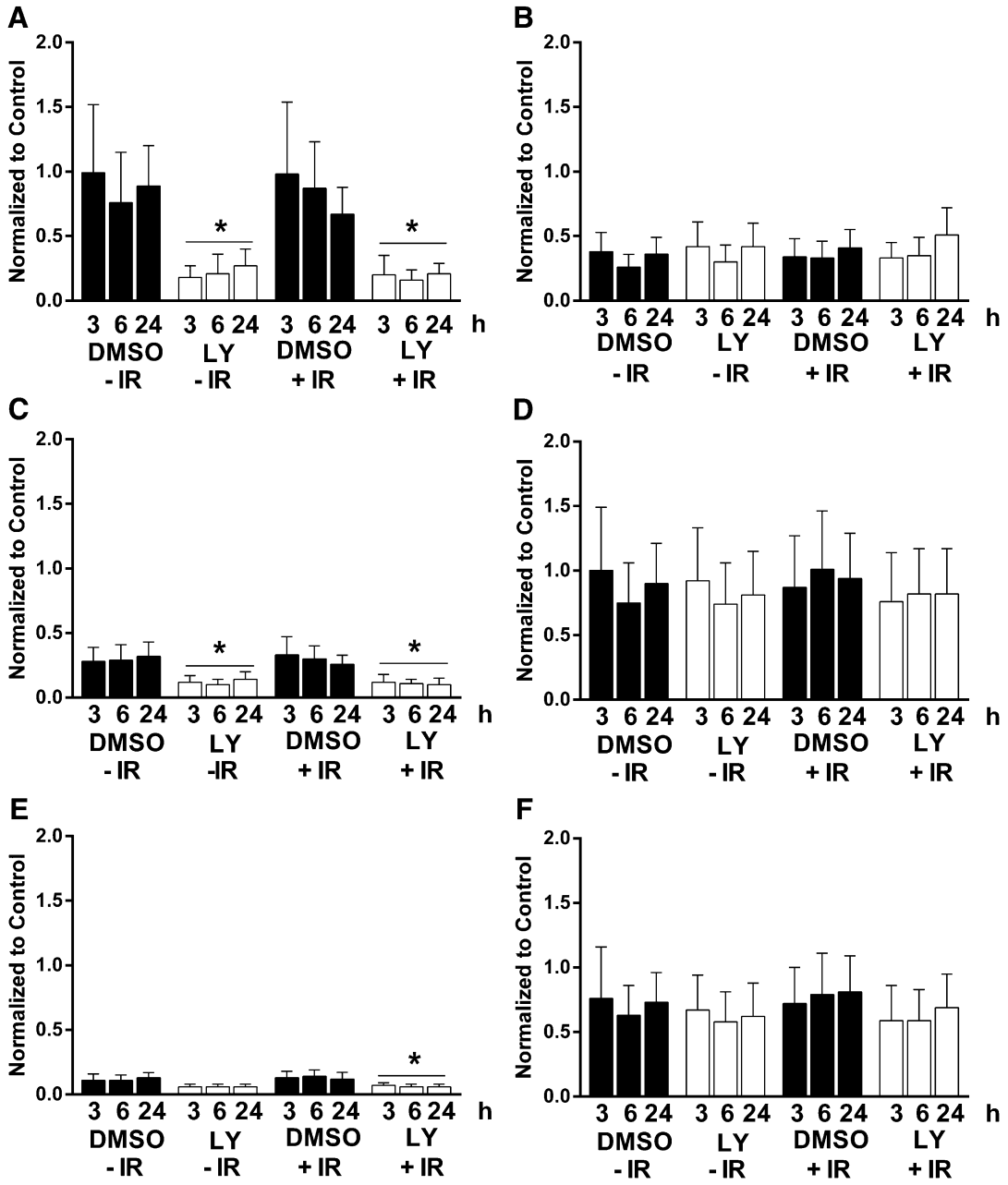

Fig. 5. Inhibition of PI3K/Akt signaling pathway by LY294002. Cells were exposed to 0 or 4 Gy IR and 1 hour later treated with vehicle or 6.25 μM LY294002 (LY). Protein lysates were generated 2, 5, or 23 hours later, and the protein content was determined by Western blotting. Quantification of relative phospho-Ser473 Akt (pAkt) (A), Akt (B), phospho-Ser21 GSK3α (pGSK3α) (C), GSK3α (D), phospho-Ser9 GSK3β (pGSK3β) (E), and GSK3β normalized to GAPDH (F). Data analyzed by ANOVA. Bars = S.E.M. $N = 5$. *$P < 0.05$ compared with DMSO-treated cells.

population to 47 ± 4%; the G_2 phase population was 4.4 ± 0.4%. The G_1-induced accumulation was transient so that by 48 hours the LY294002-treated cells had 17 ± 2% of the population in G_1 phase and 13 ± 1% in G_2 phase (Fig. 8). After γIR, however, LY294002 greatly increased the fraction of cells in G_2/M phase to 75 ± 2% at 28 hours with a marked decreased in the S phase population (11 ± 1%) (Fig. 8, A and C). By 48 hours, the G_2/M population returned to 25 ± 3% of the population, which was still elevated compared with the irradiated cells treated with the vehicle control (Fig. 8, A and C). The S phase population was 27 ± 7%.

Likewise, PX-867 (630 nM) increased the percentage of nonirradiated cells in G_1 phase at 24 and 48 hours and statistically significantly ($P < 0.05$) decreased the percentage of S phase cells to 70.2 ± 1.2% and 70.9 ± 0.3%, respectively, compared with the vehicle-treated control cell population (Fig. 9). After γIR, PX-867 also decreased the S phase population to 31.6 ± 0.9%, while producing an increase in the fraction of cells in G_2/M phase to 56.8 ± 0.9% at 24 hours (Fig. 9, A and B). At 48 hours, PX-867 continued to decrease S phase cells and increased the G_1 and G_2/M population (Fig. 9, A and C). Thus, although PX-867 was slightly less effective compared with LY294002, both inhibitors markedly reduced the S phase population in irradiated cells.

PI3K Inhibitors Reduced γIR-Induced DNA Damage. Exposure of cells to IR produces double-strand DNA breaks that rapidly result in the phosphorylation of histone H2AX on

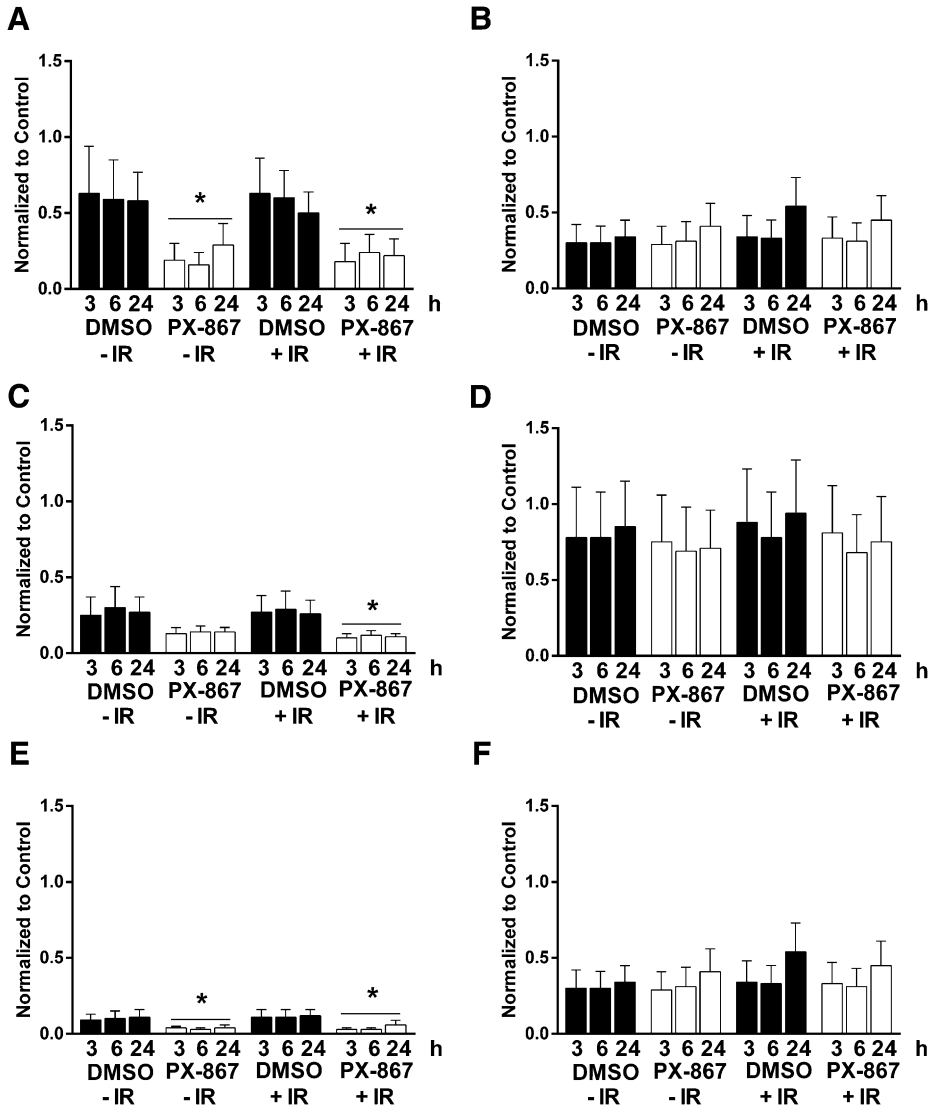

Fig. 6. Inhibition of PI3K/Akt signaling pathway by PX-867. Cells were exposed to 0 or 4 Gy IR and 1 hour later treated with vehicle or 630 nM PX-867. Protein lysates were generated 2, 5, or 23 hours later, and the protein content was determined by Western blotting. Quantification of relative phospho-Ser473 Akt (pAkt) (A), Akt (B), phospho-Ser21 GSK3α (pGSK3α) (C), GSK3α (D), phospho-Ser9 GSK3β (pGSK3β) (E), and GSK3β (F) normalized to GAPDH. Data analyzed by ANOVA. Bars = S.E.M. $N = 5$. $^*P < 0.05$ compared with DMSO-treated cells.

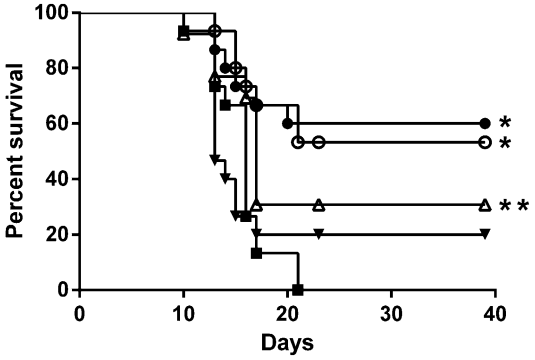

Fig. 7. In vivo radiomitigation with LY294002 and PX-867. Female C57BL/6NTac mice (15 per group) were exposed to an $LD_{50/30}$ dose (9.25 Gy) whole-body irradiation and then were injected intraperitoneally 4 hours (open symbols) or 24 hours (closed symbols) later with vehicle (■), LY294002 (30 mg/kg) (○,●), or PX-867 (30 mg/kg) (△,▼). Mice were observed for the development of the radiation-induced hematopoietic syndrome. $^*P < 0.001$. $^{**}P < 0.017$.

Ser39 to generate γH2AX, which is a reliable marker for DNA damage (Sharma et al., 2012). As anticipated, treatment of NCCIT cells with 4 Gy γIR produced a >2- to 4-fold increase in γH2AX at 3 hours (Fig. 10). Exposure to LY294002 (6.25 μM) or PX-867 (630 nM) 1 hour after 4 Gy γIR resulted in a decrease in γH2AX consistent with reduced DNA damage.

Discussion

The PI3K/Akt pathway is a central intracellular signaling conduit and essential for responses to stress and cellular damage (Abraham, 2001). The PI3K family is divided into three classes according to their structural characteristics and substrate specificity: class I, II, and III (Liu et al., 2009). The class I PI3Ks comprise class IA enzymes with a p110α, p110β, or p110δ catalytic subunit, whose activity is regulated by subunits referred collectively as p85, and class IB PI3K with a p110γ catalytic subunit, which is regulated by p84 and p87 adaptor proteins. Our previous siRNA screening results first implicated the class IA PI3K pathway because suppression of the p85α subunit resulted in radiation mitigation (Zellefrow et al., 2012). The p85α regulatory subunit facilitates the

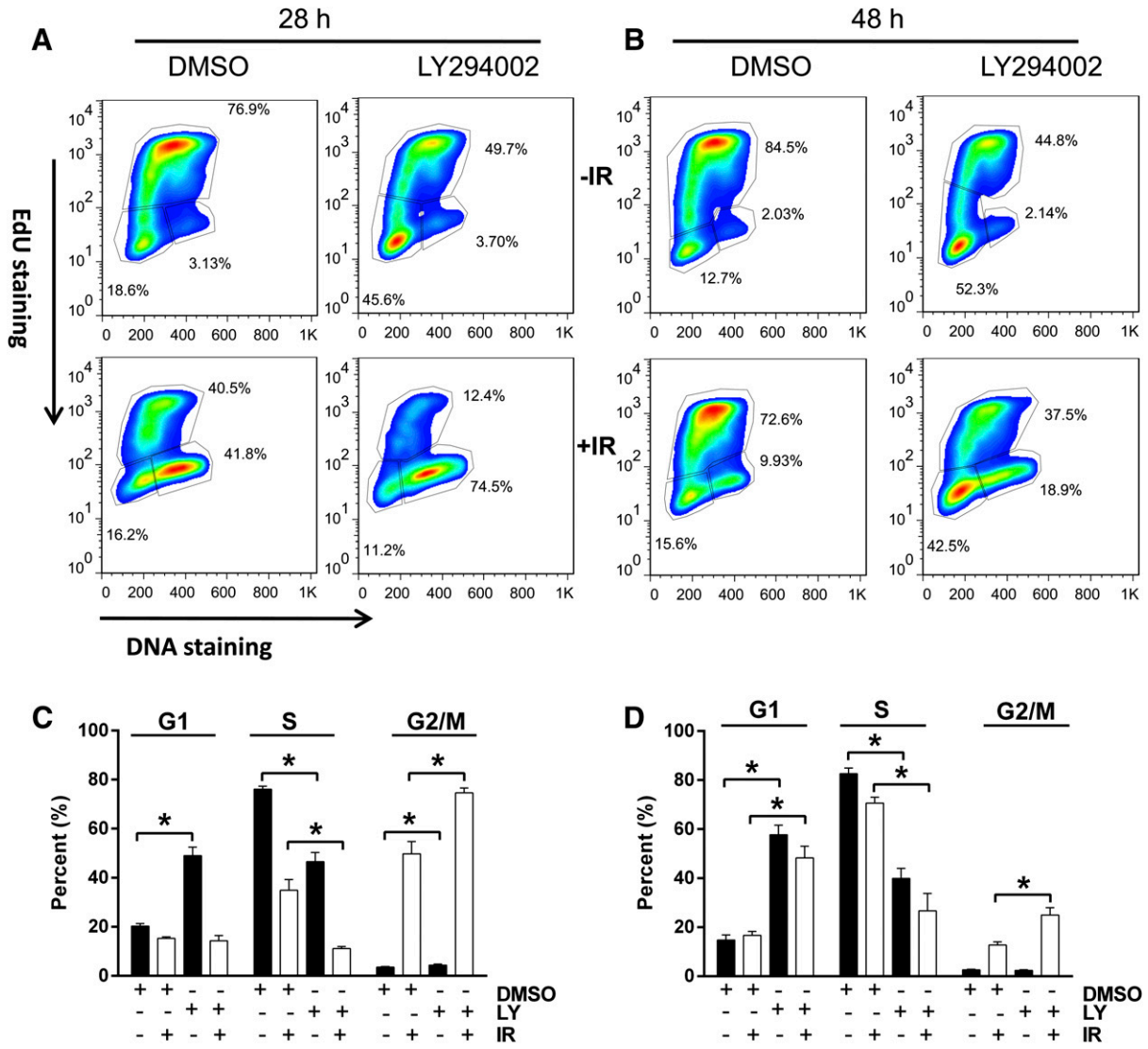

Fig. 8. Cell cycle analysis after LY294002 treatment. NCCIT cells were exposed to 0 or 4 Gy γIR, plated, incubated at 37°C for 1 hour before treatment with DMSO vehicle or LY294002 (LY) (6.25 μM). Cells were incubated for 21 or 41 hours and then treated with 10 μM 5-ethynyl-2′-deoxyuridine (EdU). After an additional 6 hours of incubation, the cells were harvested and analyzed with FACSCalibur. (A and B) Representative flow cytometry profiles. The cell cycle phases are outlined, with the upper quadrant indicating the S phase cell population, the lower right being the G_2/M phase population, and the lower left reflecting the G_1 phase cells. Quantitative cell cycle distribution 28 hours (C) or 48 hours (D) after IR exposure. Black columns indicate nonirradiated cells, and white columns indicate irradiated cells. $N = 3$. Bars = S.E.M. $^*P < 0.05$, Student's t test.

recruitment of the class IA p110 catalytic subunit to membranes after growth factor stimulation and IR stress, which then catalyzes the phosphorylation of phosphatidylinositol 4,5-bisphosphate to phosphatidylinositol 3,4,5-triphosphate and activates a wide range of distal targets, including the serine/threonine kinase Akt (Valerie et al., 2007; Liu et al., 2009).

As anticipated for a highly regulated pathway, we observed a transient PI3K activation in NCCIT cells rapidly after γIR. Intriguingly, persistent PI3K activation after γIR may occur in vivo. Suman et al. (2012), for example, recently observed elevated levels of p85α and Akt activation in mouse mammary tissues 2 and 12 months after a single total body dose of 2 Gy.

The class IA, IB, and II PI3K share a similar biochemistry but have both unique and overlapping functions that continue to be mapped (Liu et al., 2009). Genetic approaches to uncoupling the actions of specific PI3K isotypes have been frustrated by the complex and rapid coordinate regulation of these pathways. Thus, pharmacologic approaches are an appealing strategy to validate the role of the PI3K pathways because they are rapid and easily titratable. Many of the first-generation PI3K inhibitors have broad PI3K isotype activity with pleiotropic effects against other kinases, including mTOR (Knight et al., 2006; Gharbi et al., 2007). The ability to target multiple kinases can be an attractive pharmacologic attribute, especially when approaching a complex signaling network (Knight et al., 2010). The more recently synthesized compounds frequently exhibit more selectivity, although they generally retain some cross-inhibition with other protein kinases. It is noteworthy, however, that both AS-252424 and AS-605240, which have >10-fold in vitro selectivity for the class IB PI3Kγ isotype versus the α, β, or δ isotypes (Camps et al., 2005; Condliffe AM et al., 2005),

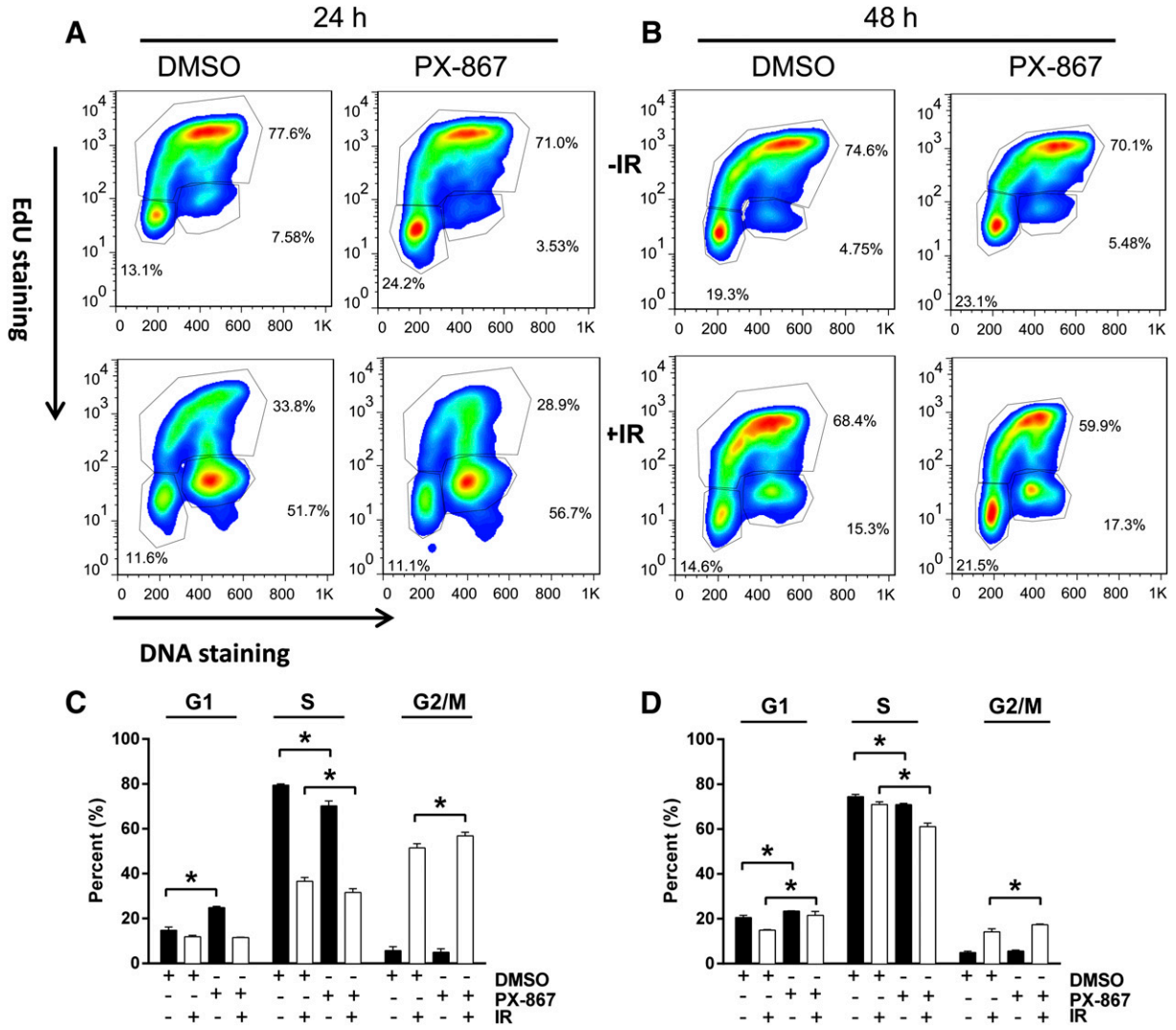

Fig. 9. Cell cycle analysis after PX-867 treatment. NCCIT cells were exposed to 0 or 4 Gy γIR, plated, incubated at 37°C for 1 hour before treatment with DMSO vehicle or PX-867 (630 nM). Cells were incubated for 17 or 41 hours and then treated with 10 μM 5-ethynyl-2′-deoxyuridine (EdU). After an additional 6 hours of incubation, the cells were harvested and analyzed with FACSCalibur. (A and B) Representative flow cytometry profiles. The cell cycle phases are outlined with the upper quadrant indicating the S phase cell population, the lower right being the G_2/M phase population and the lower left reflecting the G_1 phase cells. Quantitative cell cycle distribution 24 hours (C) or 48 hours (D) after IR exposure. Black columns indicate nonirradiated cells, and white columns indicate irradiated cells. $N = 3$. Bars = S.E.M. $^*P < 0.05$, Student's t test.

demonstrated considerable radiation mitigation activity. AS-25242 also caused radiation mitigation in NTERA2 cells (Supplemental Fig. 1F). In vivo these compounds also have anti-inflammatory activity (Camps et al., 2005; Condliffe AM et al., 2005). Examining the class IB PI3K pathway further seems warranted as several of the other pan-class IA inhibitors with radiation-mitigation effects also retain some ability to inhibit PI3Kγ, at least in vitro.

PI3K is generally considered a component of a prosurvival pathway, and inhibition of PI3K has been an attractive target for cancer therapy (Courtney et al., 2010). Indeed, there has been considerable interest in combining PI3K inhibitors with traditional cytotoxic anticancer agents (Courtney et al., 2010). Almost all of these studies, however, examine the effect of pretreatment or cotreatment of PI3K inhibitors with cytotoxic agents including γIR. Surprisingly, some investigators observed protection or the lack of sensitization to IR-induced cell death when tumor cells were either pretreated or cotreated with PI3K inhibitors (de la Peña et al., 2006; Firat et al., 2012). Thus, the PI3K inhibitors LY294002 and PI-103 were shown to protect cancer stem cells, which have an activated Akt pathway, from low γIR doses primarily by reducing apoptosis (Firat et al., 2012). In addition, rapamycin, an inhibitor of the distal PI3K/Akt target mTOR, was recently shown to protect epithelial stem cells against γIR (Iglesias-Bartolome et al., 2012) and prevent stem cell exhaustion (Laplante and Sabatini, 2012).

Nevertheless, we know very little about cellular responses when PI3K inhibitors are applied after low doses of IR, making our results about the salubrious effects of this class of compounds timely. In our initial studies on pharmacologic approaches to radiation mitigation of cell death, only a limited number of compounds were examined, and there was an absence of data concerning the biochemical disruption of the PI3K pathway (Zellefrow et al., 2012). In our current study, we documented that PI3K pathway inhibition occurs at compound concentrations that produce radiation mitigation

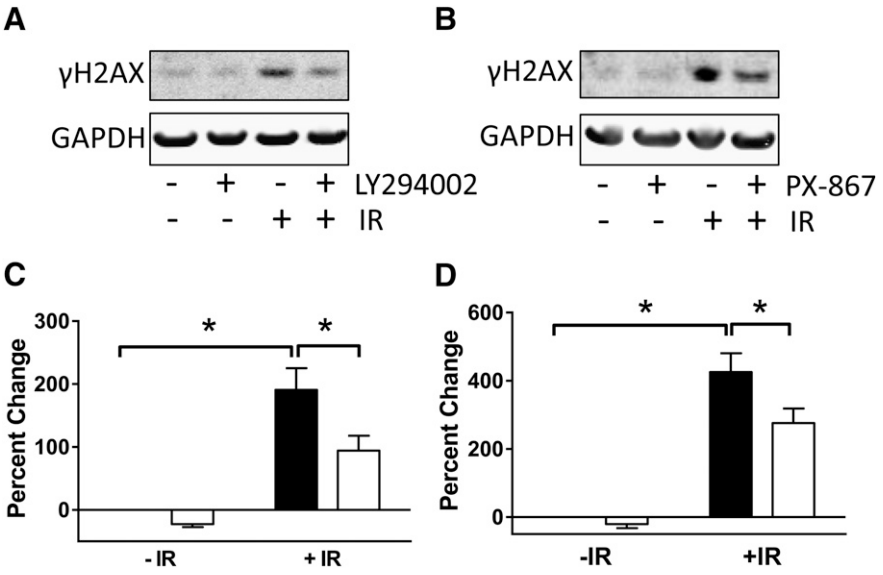

Fig. 10. Reduction of DNA damage with LY294002 and PX-867. NCCIT cells were treated with 0 or 4 Gy γIR, plated, incubated at 37°C for 1 hour before treatment with DMSO vehicle, LY294002 (6.25 μM) (A and C) or PX-867 (630 nM) (B and D) for 3 hours. (A and B) Representative Western blots of histone γH2AX Ser39 phosphorylation. (C and D) Quantification of histone γH2AX Ser39 phosphorylation. Samples were quantified from five to seven independent studies using a Li-Cor Odyssey imaging system and normalized to the levels in nonirradiated DMSO-treated cells. Bars = S.E.M. Data analyzed by two-way ANOVA. $^*P < 0.05$.

and greatly expand the number of PI3K inhibitors that share the mitigation effect. We also demonstrate for the first time in vivo radiation mitigation with PX-867.

Although increased cell survival after inhibition of a member of a survival pathway might seem somewhat paradoxical, cell stress can convert an established survival pathway into a death-mediating pathway. For example, glutamate-induced oxidative toxicity leads to an extracellular signal-regulated protein kinase (ERK)-mediated neuronal cell death that is blocked by pharmacologic inhibition of mitogen-activated protein kinase kinase 1/2 (MEK1/2) (Stanciu et al., 2000). Thus, it is important to remember the cellular context in which the pharmacologic agent is administered.

The question remains what are possible mechanisms that could contribute to the radiation mitigation. Because pAkt activation is transient and possibly completed by the time (1 hour) we added the PI3K inhibitors, it seems unlikely that radiation mitigation by PI3K inhibitors is dependent on chronic elevation of pAkt. Somatic cells respond to DNA damage by activating sets of discrete checkpoint pathways, most importantly the G_1 checkpoint, while mammalian pluripotent cells do not generally undergo G_1 growth arrest after DNA damage and exploit other DNA damage checkpoints to allow proper repair before cytokinesis (Wang et al., 2009; Sokolov et al., 2011). Previous studies (Mitchell et al., 2010) have revealed cell cycle arrest after insulin-like growth factor-1 (IGF1) pretreatment leads to the engagement of a G_2/M checkpoint that protects acinar cells from radiation-induced apoptosis, possibly allowing time for DNA repair. Consistent with this notion of alternative checkpoint engagement, we observed a marked increase in G_2/M arrest in the NCCIT cells after 4 Gy in the absence of a fully functional G_1 phase arrest (Figs. 8 and 9). This absence of a G_1 checkpoint increases the importance of other DNA damage checkpoints to preserve genomic integrity.

When compared with somatic cells, pluripotent stem cells have distinctive proliferative properties, which include an atypical cell cycle primarily composed of S and M phases with relatively limited gap phases, which may render them differentially sensitive to the cellular damage associated with IR (Burdon et al., 2002). Pluripotent cells also engage in apoptosis, the most common form of programmed cell death, as a protective mechanism, presumably to prevent cells containing extensively damaged genomes from contributing during development or tissue regeneration. The decrease in the S phase population observed with PI3K inhibition may enable repair before DNA replication or cytokinesis and would likely contribute to the decrease in apoptosis after IR. This topic is worthy of additional investigation.

We found that NCCIT cells, similar to other cells (Gewirtz et al., 2008), undergo some senescence after IR, as revealed by an increase in senescence-associated β-galactosidase. However, this was not significantly altered after treatment with LY294002 (data not shown), adding further support for the importance of the effects on apoptosis.

Our chemical clustering also revealed other potential molecular targets, notably ACE, HMG-CoA reductase, and glutamate receptors. It is interesting that our previous siRNA screen found both angiotensin and glutamate pathway involvement, although we did not observe any evidence for HMG-CoA pathway participation (Zellefrow et al., 2012). There are a number of reasons for the lack of effect with siRNA, including poor transfection of siRNA or a prolonged half-life of the targeted mRNA. Nonetheless, our current study reveals an advantage of a combined computational and small molecule approach.

In summary, our observation with multiple PI3K inhibitors provides encouragement that pharmacologic approaches aimed at mitigating IR-mediated death should be pursued further. The sizable number of available inhibitors for the PI3K/Akt pathway, many of which are in human clinical trials, provides a potentially valuable resource to further interrogate this hypothesis.

Authorship Contributions

Participated in research design: Lazo, Sharlow, Epperly, Wipf, Greenberger.

Conducted experiments: Sharlow, Epperly, Lira, Leimgruber, Skoda.

Contributed new reagents or analytic tools: Sharlow, Skoda, Wipf.

Performed data analysis: Lazo, Sharlow, Epperly, Lira, Leimgruber, Skoda, Wipf.

Wrote or contributed to the writing of the manuscript: Lazo, Sharlow, Epperly, Skoda, Wipf, Greenberger.

References

Abraham RT (2001) Cell cycle checkpoint signaling through the ATM and ATR kinases. *Genes Dev* **15**:2177–2196.

Brognard J, Clark AS, Ni Y, and Dennis PA (2001) Akt/protein kinase B is constitutively active in non-small cell lung cancer cells and promotes cellular survival and resistance to chemotherapy and radiation. *Cancer Res* **61**:3986–3997.

Burdon T, Smith A, and Savatier P (2002) Signalling, cell cycle and pluripotency in embryonic stem cells. *Trends Cell Biol* **12**:432–438.

Camps M, Rückle T, Ji H, Ardissone V, Rintelen F, Shaw J, Ferrandi C, Chabert C, Gillieron C, and Françon B, et al. (2005) Blockade of PI3Kγ suppresses joint inflammation and damage in mouse models of rheumatoid arthritis. *Nat Med* **11**: 936–943.

Citrin D, Cotrim AP, Hyodo F, Baum BJ, Krishna MC, and Mitchell JB (2010) Radioprotectors and mitigators of radiation-induced normal tissue injury. *Oncologist* **15**:360–371.

Condliffe AM, Davidson K, Anderson KE, Ellson CD, Crabbe T, Okkenhaug K, Vanhaesebroeck B, Turner M, Webb L, and Wymann MP, et al. (2005) Sequential activation of class IB and class IA PI3K is important for the primed respiratory burst of human but not murine neutrophils. *Blood* **106**:1432–1440.

Courtney KD, Corcoran RB, and Engelman JA (2010) The PI3K pathway as drug target in human cancer. *J Clin Oncol* **28**:1075–1083.

de la Peña L, Burgan WE, Carter DJ, Hollingshead MG, Satyamitra M, Camphausen K, and Tofilon PJ (2006) Inhibition of Akt by the alkylphospholipid perifosine does not enhance the radiosensitivity of human glioma cells. *Mol Cancer Ther* **5**: 1504–1510.

Epperly MW, Franicola D, Shields D, Rwigema JC, Stone B, Zhang X, McBride W, Georges G, Wipf P, and Greenberger JS (2010) Screening of antimicrobial agents for in vitro radiation protection and mitigation capacity, including those used in supportive care regimens for bone marrow transplant recipients. *In Vivo* **24**:9–19.

Firat E, Weyerbrock A, Gaedicke S, Grosu AL, and Niedermann G (2012) Chloroquine or chloroquine-PI3K/Akt pathway inhibitor combinations strongly promote γ-irradiation-induced cell death in primary stem-like glioma cells. *PLoS ONE* **7**: e47357.

Gewirtz DA, Holt SE, and Elmore LW (2008) Accelerated senescence: an emerging role in tumor cell response to chemotherapy and radiation. *Biochem Pharmacol* **76**: 947–957.

Gharbi SI, Zvelebil MJ, Shuttleworth SJ, Hancox T, Saghir N, Timms JF, and Waterfield MD (2007) Exploring the specificity of the PI3K family inhibitor LY294002. *Biochem J* **404**:15–21.

Greenberger JS, Clump D, Kagan V, Bayir H, Lazo JS, Wipf P, Li S, Gao X, and Epperly MW (2011) Strategies for discovery of small molecule radiation protectors and radiation mitigators. *Front Oncol* **1**:59.

Hall EJ and Giaccia AJ (2006) *Radiobiology for the Radiologist*, Lippincott Williams & Wilkins, Philadelphia, PA.

Iglesias-Bartolome R, Patel V, Cotrim AP, Leelahavanichkul K, Molinolo AA, Mitchell JB, and Gutkind JS (2012) mTOR inhibition prevents epithelial stem cell senescence and protects from radiation-induced mucositis. *Cell Stem Cell* **11**: 401–414.

Johnson SM, Torrice CD, Bell JF, Monahan KB, Jiang Q, Wang Y, Ramsey MR, Jin J, Wong KK, and Su L, et al. (2010) Mitigation of hematologic radiation toxicity in mice through pharmacological quiescence induced by CDK4/6 inhibition. *J Clin Invest* **120**:2528–2536.

Kim H, Bernard ME, Flickinger J, Epperly MW, Wang H, Dixon TM, Shields D, Houghton F, Zhang X, and Greenberger JS (2011) The autophagy-inducing drug carbamazepine is a radiation protector and mitigator. *Int J Radiat Biol* **87**: 1052–1060.

Kim SO, Bolton EE, and Bryant SH (2012) Effects of multiple conformers per compound upon 3-D similarity search and bioassay data analysis. *J Cheminform* **4**:28.

Knight ZA, Gonzalez B, Feldman ME, Zunder ER, Goldenberg DD, Williams O, Loewith R, Stokoe D, Balla A, and Toth B, et al. (2006) A pharmacological map of the PI3-K family defines a role for p110α in insulin signaling. *Cell* **125**: 733–747.

Knight ZA, Lin H, and Shokat KM (2010) Targeting the cancer kinome through polypharmacology. *Nat Rev Cancer* **10**:130–137.

Laplante M and Sabatini DM (2012) mTOR signaling in growth control and disease. *Cell* **149**:274–293.

Liu P, Cheng H, Roberts TM, and Zhao JJ (2009) Targeting the phosphoinositide 3-kinase pathway in cancer. *Nat Rev Drug Discov* **8**:627–644.

Ma C, Lazo JS, and Xie X-Q (2011) Compound acquisition and prioritization algorithm for constructing structurally diverse compound libraries. *ACS Comb Sci* **13**: 223–231.

Mitchell GC, Fillinger JL, Sittadjody S, Avila JL, Burd R, and Limesand KH (2010) IGF1 activates cell cycle arrest following irradiation by reducing binding of ΔNp63 to the p21 promoter. *Cell Death Dis* **1**:e50.

Moulder JE, Cohen EP, and Fish BL (2011) Captopril and losartan for mitigation of renal injury caused by single-dose total-body irradiation. *Radiat Res* **175**:29–36.

Olson CF (1995) Parallel algorithms for hierarchical clustering. *Parallel Comput* **21**: 1313–1325 DOI: 10.1016/0167-8191(95)00017-I.

Rwigema JC, Beck B, Wang W, Doemling A, Epperly MW, Shields D, Goff JP, Franicola D, Dixon T, and Frantz MC, et al. (2011) Two strategies for the development of mitochondrion-targeted small molecule radiation damage mitigators. *Int J Radiat Oncol Biol Phys* **80**:860–868.

Sharma A, Singh K, and Almasan A (2012) Histone H2AX phosphorylation: a marker for DNA damage. *Methods Mol Biol* **920**:613–626.

Sokolov MV, Panyutin IV, Panyutin IG, and Neumann RD (2011) Dynamics of the transcriptome response of cultured human embryonic stem cells to ionizing radiation exposure. *Mutat Res* **709-710**:40–48.

Stanciu M, Wang Y, Kentor R, Burke N, Watkins S, Kress G, Reynolds I, Klann E, Angiolieri MR, and Johnson JW, et al. (2000) Persistent activation of ERK contributes to glutamate-induced oxidative toxicity in a neuronal cell line and primary cortical neuron cultures. *J Biol Chem* **275**:12200–12206.

Suman S, Johnson MD, Fornace AJ, Jr, and Datta K (2012) Exposure to ionizing radiation causes long-term increase in serum estradiol and activation of PI3K-Akt signaling pathway in mouse mammary gland. *Int J Radiat Oncol Biol Phys* **84**: 500–507.

Thaker NG, McDonald PR, Zhang F, Kitchens CA, Shun TY, Pollack IF, and Lazo JS (2010) Designing, optimizing, and implementing high-throughput siRNA genomic screening with glioma cells for the discovery of survival genes and novel drug targets. *J Neurosci Methods* **185**:204–212.

Valerie K, Yacoub A, Hagan MP, Curiel DT, Fisher PB, Grant S, and Dent P (2007) Radiation-induced cell signaling: inside-out and outside-in. *Mol Cancer Ther* **6**: 789–801.

Viniegra JG, Martínez N, Modirassari P, Hernández Losa J, Parada Cobo C, Sánchez-Arévalo Lobo VJ, Aceves Luquero CI, Alvarez-Vallina L, Ramón y Cajal S, and Rojas JM, et al. (2005) Full activation of PKB/Akt in response to insulin or ionizing radiation is mediated through ATM. *J Biol Chem* **280**:4029–4036.

Wang XQ, Lui VC, Poon RTP, Lu P, and Poon RYC (2009) DNA damage mediated s and g(2) checkpoints in human embryonal carcinoma cells. *Stem Cells* **27**:568–576.

Welsch ME, Snyder SA, and Stockwell BR (2010) Privileged scaffolds for library design and drug discovery. *Curr Opin Chem Biol* **14**:347–361.

Wipf P and Halter RJ (2005) Chemistry and biology of wortmannin. *Org Biomol Chem* **3**:2053–2061.

Wipf P, Minion DJ, Halter RJ, Berggren MI, Ho CB, Chiang GG, Kirkpatrick L, Abraham R, and Powis G (2004) Synthesis and biological evaluation of synthetic viridins derived from C(20)-heteroalkylation of the steroidal PI-3-kinase inhibitor wortmannin. *Org Biomol Chem* **2**:1911–1920.

Zellefrow CD, Sharlow ER, Epperly MW, Reese CE, Shun T, Lira A, Greenberger JS, and Lazo JS (2012) Identification of druggable targets for radiation mitigation using a small interfering RNA screening assay. *Radiat Res* **178**:150–159.

Address correspondence to: John S. Lazo, Department of Pharmacology, P.O. Box 800793, University of Virginia, Charlottesville, VA 22908-0793. E-mail: lazo@virginia.edu